ACS Partner Journal

CHEMICAL & BIOMEDICAL IMAGING

Open Access

This article is licensed under CC-BY-NC-ND 4.0

pubs.acs.org/ChemBioImaging

Article

Milk Exosome-Glow Nanosystem for Cancer Cellular and Tissue Bioimaging

Nycol M. Cotto,[§] Neeraj Chauhan,[§] Benilde Adriano, Deepak S. Chauhan, Marco Cabrera, Subhash C. Chauhan, and Murali M. Yallapu*

Cite This: *Chem. Biomed. Imaging* 2024, 2, 711−720

Read Online

ACCESS | Metrics & More | Article Recommendations

ABSTRACT: Milk-derived exosomes are widely used for diagnosis, delivery, imaging, and theranostic applications. Near-Infrared (NIR) based fluorescence bioimaging is an attractive and safer technique that is used for clinical applications. However, almost all NIR imaging agents tend to have poor photostability, short half-life, nonspecific protein binding, and concentration-dependent aggregation(s). Therefore, there is an unmet clinical need to develop newer and safer modalities to package and deliver NIR imaging agents. Bovine milk exosomes are natural, biocompatible, safe, and efficient nanocarriers that facilitate the delivery of micro- and macromolecules. Herein, we developed an exosome-based NIR dye loaded nanoimaging formulation that offers improved solubility and photostability of NIR dye. Following the acetic acid based extracellular vesicle (EV) treatment method, we extracted the bovine milk exosomes from a variety of pasteurized grade milk. The EVs were screened for their physicochemical properties such as particle size and concentration and zeta potential. The stability of these exosomes was also determined under different conditions, including storage temperatures, pH, and salt concentrations. Next, indocyanine green, a model NIR dye was loaded into these exosomes (Exo-Glow) via a sonication method and further assessed for their improved fluorescence intensity and photostability using an IVIS imaging system. Initial screening suggested that size of the selected bovine milk exosomes was ∼100−135 nm with an average particle concentration of 5.8 × 10^2 particles/mL. Exo-Glow further demonstrated higher fluorescence intensity in cancer cells and tissues when compared to free dye. These results showed that Exo-Glow has the potential to serve as a safer NIR imaging tool for cancer cells/tissues.

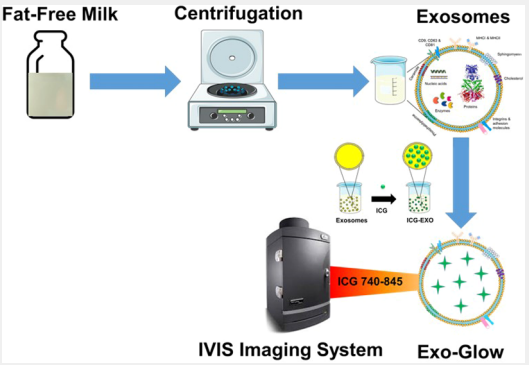

KEYWORDS: *Bioimaging, Optical Imaging, NIR fluorescence, ICG, Exosomes, Nanocarriers*

INTRODUCTION

Near-infrared (NIR) fluorescence imaging is one of the most innovative technologies for cells and tissue bioimaging because it can minimize tissue background interference, allowing it to produce more sensitive and in-depth visualization. This is due to its wavelength range of 700−1000 nm that allows it to have a low absorption and autofluorescence.[1−3] Efficient NIR imaging needs to have ideal chemical and photophysical properties such as intense fluorescence, photostability, and good aqueous solubility. However, many of the NIR dyes have a series of limitation such as poor hydrophilicity and photostability, low intensity, and short half-life.[4] Among several NIR dyes, indocyanine green (ICG)[5] is an U.S. Food and Drug Administration (FDA) approved tricarbocyanine fluorescent NIR dye as an indicator of cardiac output, hepatic function and liver blood flow, and ophthalmic angiography.[6] ICG exhibits a strong imaging potential due to its high signal-to-background ratio.[7,8] ICG-based NIR fluorescent (NIRF) imaging is an attractive and safer techniques used in various clinical applications. However, ICG tends to have poor photostability, short half-life, nonspecific proteins binding, and concentration-dependent aggregation.[9] Therefore, there is an unmet clinical need to develop newer modalities to package and deliver ICG. One potentially safe way to overcome these issues is the use of nanocarriers to package ICG. To date a number of nanosystems that have been developed for encapsulating therapeutic and imaging materials such as polymeric, iron oxide, liposomal, and others.[10]

Exosomes are one type of extracellular vesicles (EV) and are composed of biomolecular lipid-bilayer nanostructures that are released by all cells.[11−13] Exosomes with an average size of 30−150 nm can serve as transporters of a variety of molecules such as proteins, lipids, mRNAs, and RNA.[14] Exosomes can be

Received: April 26, 2024
Revised: July 25, 2024
Accepted: July 26, 2024
Published: August 7, 2024

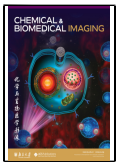

ACS Publications

© 2024 The Authors. Co-published by Nanjing University and American Chemical Society

released by cells, tissues, and biological fluids such as blood, milk, and urine.[12] Exosomes have the potential to be a naturally occurring delivery system because of their long circulating half-life, biocompatibility, as well as minimum toxicity and tumor targeting abilities.[15]

There are a variety of exosomes that are extracted from natural sources, and there's been an increase in the study of these as natural nanoplatforms for drug delivery and imaging agents. One example of an exosome derived from natural sources are milk exosomes.[16,17] Bovine milk exosomes are composed of miRNAs and other molecules of milk proteins like casein, β-lactoglobulin, miR-101, and miR-150.[18,19] Bovine milk exosomes contain 2107 proteins[20] and are involved with vesicle fusion as well as possible intercellular signaling.[21] Therefore, considering bovine milk exosomes natural, biocompatible, safe, and efficient nanocarriers that facilitate the delivery of micro and macro molecules, we seek to develop an exosome based NIR dye (ICG) loaded imaging system that offers improved solubility, photostability, and imaging capabilities.

MATERIALS AND METHODS

Chemicals, Chicken Breast, and Bovine Milk Samples

Acetic acid (A6283), sodium chloride (S7653), acetone (270725), and ICG (1340009) were purchased from Sigma-Aldrich (St. Louis, MO, USA). All other laboratory solvents, reagents, chemicals, and cell culture plastics were purchased from Fisher Scientific (Pittsburgh, PA, USA) or Sarstedt, Inc. (Newton, NC, USA). Chicken breast tissues and various bovine milk samples used in this study were purchased from a local HEB and Walmart grocery stores and kept at 4 °C during usage and/or until the expiration date. Milk samples were as follows: 5 different brands (all 0%) as Horizon Organic, HEB Organics Central Market, HEB Fat Free, Great Value Fat Free, Oak Farms Dairy-Dairy Pure, and 4 different fat percentages (0%, 1%, 2%, and 3%) of Horizon Organic Milk.

Isolation of EVs

For the removal of milk fat globules and other debris and contaminants, milk samples (25 mL) were centrifuged at 2000 rcf for 20 min with a temperature of 4 °C using a Rotor S-4 x Universal-Large with a Centrifuge 5920 R (Eppendorf AG, Germany). Supernatant containing the defatted milk was collected for acetic acid treatment.[22]

Acetic acid (AA) Treatment

The supernatant (15 mL) was warmed up at 37 °C using a hot plate for 10 min, and acetic acid (15 mL) was slowly added while mixture was stirring at 500 rpm. The treated sample was stirred for 5 min and later centrifuged at 4198 rcf for 20 min at 25 °C. This centrifugation allowed for separation of the casein (pellet) and whey (supernatant).[23] Supernatant was collected, subjected to ultracentrifugation, washed with Phosphate-Buffered Solution (PBS), and stored at 4 °C for further studies.[24] Exosomes were lyophilized using a freeze-dryer (Labconco, Kansas City, MI, USA) to determine the weight of the EVs for future studies.

Particle Size, Concentration, and Zeta Potential

To measure the particle size, particle distribution, and concentration of exosomes, 150 μL of exosomes was dispersed in 3 mL of MilliQ ultrapure water and sonicated for 50 s using the VirSonic Ultrasonic Cell Disrupter 100 (200 W, The VirTis Company, Gardiner, NY, USA). Sonication allowed uniform suspension of particles in the solution which was placed in a clear plastic cuvette (DTS0012), and the Malvern Zetasizer Ultra instrument (Nano ZS, Malvern Instruments, Malvern, UK) was used to measure particle size and concentration characteristics using the dynamic light scattering (DLS) principle.[25] A total of 3 readings were collected for each sample. For zeta potential, 50 μL of sample was mixed with 1 mL of 1× PBS and sonicated for 50 s, this solution was further placed on a Folded Capillary Zeta Cell (DTS 1070, Malvern Instruments, Malvern UK) and surface charge (zeta potential) was measured using Malvern Zetasizer Ultra instrument.

Physical Stability

To assess the physical stability of the extracted exosomes, particle size measurements were performed using the DLS system as mentioned above, under various physical environmental conditions such as different pH (2, 3, 6, 7, 7.4 and 8), salinity (0.10%, 0.25%, 0.50%, 0.75%, 0.90% and 1% NaCl), and temperature (4, 25, 27, 30, 35, 37, and 40 °C).[26]

ICG Loading into Exosomes

Bovine milk extracted exosomes were loaded with ICG dye through a physical encapsulation method, sonication.[27] Briefly, a master stock solution of ICG dye was prepared at a 5 mg/mL concentration in water. Next, from the master stock dye solution, 1 mg of dye was loaded to 10 mg of exosomes by placing these solutions on ice and sonicating for 30 s, 5 times with a 2 min rest between sonication cycles. Further, the dialysis tubing method was employed to remove free (unbound) dye. Briefly, freshly prepared 1 mL of 100 μg ICG loaded exosomes were transferred into a dialysis tube (SnakeSkin Dialysis Tubing, 3.5 kDa MWCO, 22 mm, Fisher Scientific, Waltham, MA, USA) and placed in a beaker with 500 mL ultrapure Milli-Q water. The beaker was then kept for stirring at 150 rpm at 37 °C. Water outside the dialysis tube was replaced every 30 min until 6 h, and the content inside the tubing was analyzed with a UV−vis spectrophotometer (Varioskan LUX Multimode Microplate Reader) to measure the ICG in exosomes. Results indicated that ∼92% dye loading was obtained into the exosomes, and working dilutions/concentrations (5, 7.5, 10, 15, and 20 μg) for ICG loaded exosomes (ICG-EXO) for further studies were calculated accordingly.

Biochemical Characterization of ICG-EXO

The biochemical characterization of ICG-EXO was evaluated by spectral analyses[28] confirmed from its absorption profiles at different concentrations (5−20 μg). For this, freshly prepared ICG-EXO was analyzed in a black 96-well microplate at room temperature, and spectra were obtained at 300−900 nm by utilizing a UV−vis spectrophotometer (Varioskan LUX Multimode Microplate Reader, Thermo Fisher Scientific, Waltham, MA, USA). Data were further analyzed by using the built-in software Skanlt RE 6.02.

Fluorescence Optical Imaging

Drops (5 μL) of different dilutions (5, 7.5, 10, 15, and 20 μg) of free ICG dye and ICG-EXO were placed on filter paper (GE Healthcare Whatman, Diameter 125 mm Cat No. 1001−125). Upon drying, filter papers were imaged using an IVIS Spectrum In Vivo Imaging System (PerkinElmer, Waltham, MA, USA).[29] Emission and excitation ranges for ICG were 780−845 nm. A similar protocol was followed for *ex vivo* imaging of free ICG and ICG-EXO on chicken breast at 0 and 24 h after placing the drops onto the breast tissues. Additionally, the stability and penetration capability of ICG dye and ICG-EXO were examined with 2% agarose solutions (for thick tissue mimicking) mixed with different concentrations of free and exosomal dye in glass vials.

Hemocompatibility

A hemolysis (hemocompatibility) assay was performed to determine the biosafety profile of dye loaded bovine milk exosomes.[29] For this, human red blood cells (RBCs) were collected by centrifuging 10 mL of single donor human whole blood (IWB1K2E10 ML, Innovative Research, Inc., Novi, MI, USA) at 2000 rpm for 10 min. RBC pellets were then resuspended in 10 mL of RPMI-1640 phenol red free growth media. Next, 100 μL of RBCs was incubated with different concentrations of free ICG dye and ICG-EXO (5, 10, 25, 50, 75, 100, and 200 μg) for 2 h at 37 °C in 1.5 mL Eppendorf tubes, maintaining the tubes in a standing position. After the indicated end point, samples were centrifuged at 1000 rpm for 5 min and the RBC pellet after centrifugation was used for observing morphological changes as the result of the lysing phenomenon. For this, a drop of 10 μL of

https://doi.org/10.1021/cbmi.4c00040
Chem. Biomed. Imaging 2024, 2, 711−720

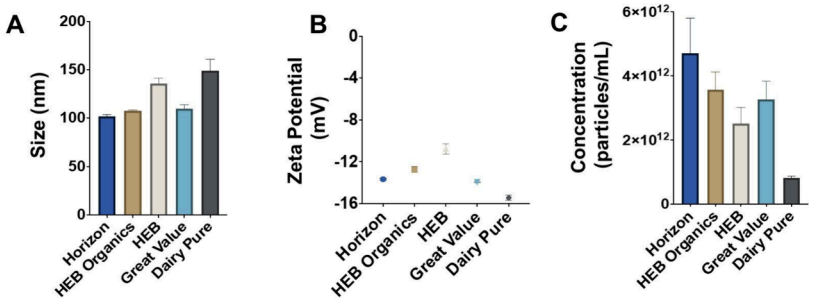

Figure 1. Physicochemical characterization of five different brand milk derived exosomes. Exosomes were extracted from five different brands of milk with 0% fat content. (A) Particle size, (B) zeta potential, and (C) particle concentrations were measured by DLS, and measurements were taken in triplicate. Data represents the average of three individual experiments. Error bars show SEM, $n = 3$.

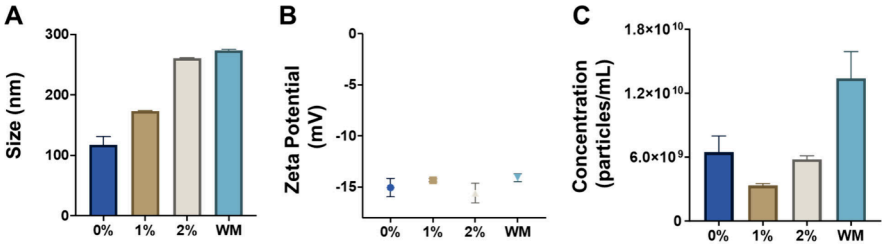

Figure 2. Physicochemical characterization of varied fat content milk derived exosomes. Exosomes were extracted from four different degrees of fat (0%, 1%, 2%, and whole fat) containing milk. (A) Particle size, (B) zeta potential, and (C) particle concentration as measured by DLS, and measurements were taken in triplicate. Data represents the average of three individual experiments. Error bars show SEM, $n = 3$.

pellet was placed onto a glass slide and smeared using another spare slide at 30° angel. Slides were then imaged with a bright-field microscope (EVOS M7000, Invitrogen, Thermo Fisher Scientific, MA, USA). In this experiment, sodium dodecyl sulfate (SDS) and phosphate buffered saline (PBS) were used as positive and negative controls, respectively.

Cellular Biocompatibility

The cellular biocompatibility of ICG loaded exosomes was determined with the MCF-7 (breast cancer, purchased from ATCC, Manassas, VA, USA) cell line by using a CellTiter96 Aqueous One Solution [3-(4,5-dimethylthiazol-2-yl)-5-(3-carboxymethoxyphenyl)-2-(4-sulfophenyl)-2H-tetrazolium, inner salt] MTS assay (Promega, Madison, WI, USA)].[29] Briefly, 5000 cells per well were plated in 96-well plates and allowed to attach overnight. The next morning, cells were exposed to various concentrations of free ICG and ICG-EXO (5, 10, 25, 50, 75, 100, and 200 μg) for another 24 h. At the end of this time point, 20 μL/well MTS reagent was added, and plates were incubated at 37 °C for 4 h. Further, absorbance (optical density) was recorded at 490 nm, and data was normalized to nontreated cells used as controls. The experiment was performed three individual times in replicates of 6.

Cellular Binding

Two breast cancer cell lines (MCF-7 and MDA-MB 231, purchased from ATCC, Manassas, VA, USA) were seeded at a density of 50,000 cells/chamber in 4-chamber slides and allowed to adhere overnight. The next day, cells were treated with10 μg of either free ICG or ICG-EXO for 3 h. Further, slides were carefully washed with 1× PBS 3 times, fixed with 4% paraformaldehyde for 20 min at room temperature, coverslipped using the mounting medium, and stored at 4 °C for complete drying minimum for 1 day prior to imaging. Cells were then imaged for ICG binding using an EVOS M7000 fluorescent microscope under the CY7 channel at 200×.

In Situ Tumor Specific Binding

Immunohistochemistry (IHC) technique was utilized to analyze the binding affinity of free ICG and ICG-EXO using breast cancer (no. BR087e) tissue microarrays (TMAs) (US Biomax, Inc., Derwood, MD, USA), containing normal and malignant human tissues. Briefly, slides were deparaffinized at 64 °C on a heating plate for 2 h and in a xylene wash for 10 min. Next, slides were rehydrated with different concentrations of alcohol content (100% for 10 min and 90%, 70%, 50% and 30% for 5 min each) followed by antigen retrieval and blocking. TMAs were then exposed to free ICG and ICG-EXO overnight at a concentration of 100 μg/mL. The next day, slides were washed with 1× TBS 3 times for 10 min each and followed by imaging utilizing a fluorescent microscope (EVOS M7000) under CY7 channel at 40×.

Statistical Analysis

All the data was expressed as mean ± standard error of mean (SEM). The statistical significance among treatments was determined using the one-way ANOVA Test (GraphPad Prism 10.1.2). A p-value < 0.05 was considered significant.

RESULTS

Optimization and Physicochemical Characterization of Bovine Milk Exosomes

We screened 5 different brands of 0% (fat free) milk, namely, Horizon Organic, HEB Organics, HEB Fat Free, Great Value, and Dairy Pure to extract ideal exosomes to serve as carriers to deliver NIR dye for bioimaging purposes. The 5 brands of fat-free milk were analyzed to determine particle size distribution, charge, and particle concentration. The particle size of exosomes derived from Horizon, HEB Organics, HEB Milk, Great Value, and Dairy Pure exhibited as 133.43 ± 2.8, 109.04 ± 3.73, 159.86 ± 11.66, 128.49 ± 7.48, and 153.71 ± 2.61 nm, respectively (Figure 1A). The zeta potential of exosomes derived from Horizon and Great Value milks had an average of ∼ −14 mV, HEB Organics milk had a zeta potential of ∼ −13 mV, HEB milk had a zeta potential of ∼ −11 mV, while Dairy Pure milk showed a zeta potential of ∼ −15 mV (Figure 1B). Based on the exosomal particle size average (116.71 ± 3.33 nm), it was determined that Horizon milk had the smallest range of variability and provided the most consistent values. Regarding particle concentration, Horizon milk (4.7×10^{12}

https://doi.org/10.1021/cbmi.4c00040
Chem. Biomed. Imaging 2024, 2, 711−720

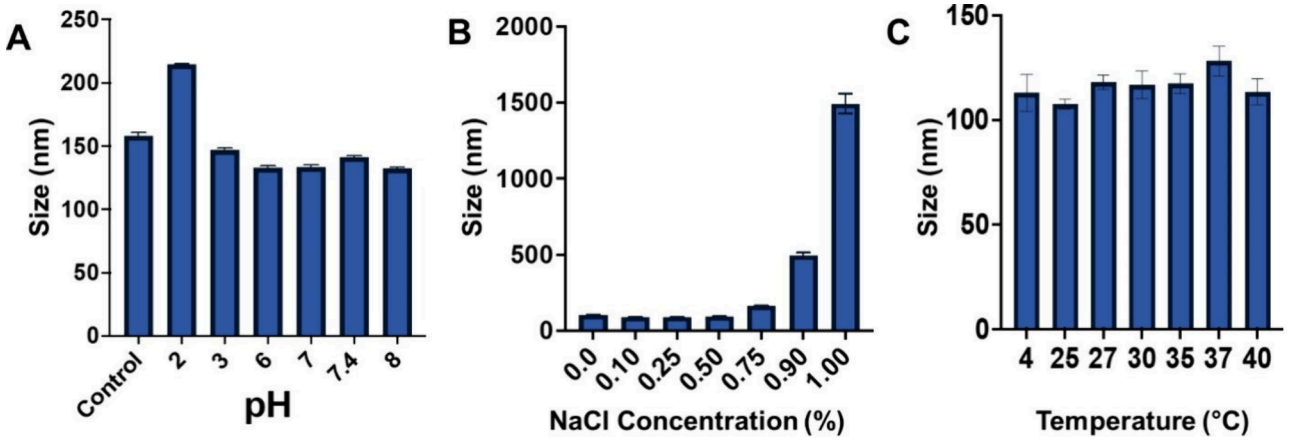

Figure 3. Physical stability of milk exosomes. Based on size consistency, fat free Horizon milk was selected to measure the stability of vesicles under different (A) pH, (B) NaCl salt concentrations, and (C) temperatures. The graphs represent the averages of three individual experiments. Error bars show SEM, $n = 3$.

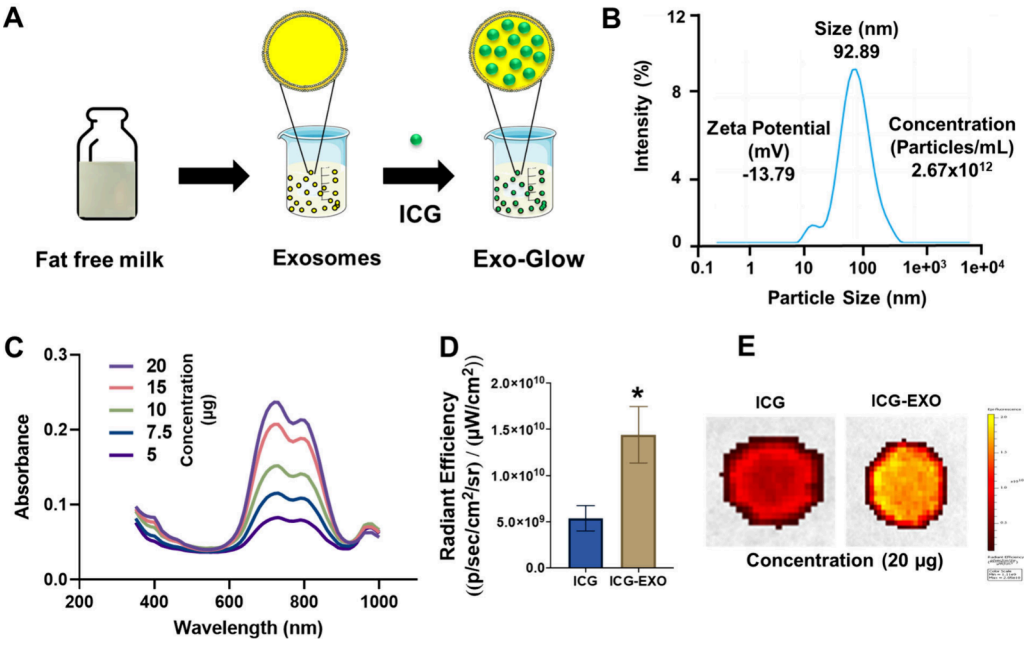

Figure 4. Characterization of ICG-EXO formulation. (A) Schematic illustration of preparation of ICG-EXO formulation. (B) ICG was loaded into the exosomes and particle size distribution, particle concentration, and zeta potential were measured by DLS. (C) UV−vis spectra of ICG-EXO at different concentrations. (D,E) Fluorescence intensity was measured using an IVIS imaging system. Bar graphs represent the quantitative analysis of fluorescence signal (intensity) ROI (radiation efficiency = photons/s/cm^2/sr) of free ICG and its loaded exosomes. Data represents the average of three individual experiments. Error bars show SEM, $n = 3$. *$p < 0.05$. A formulation with a final concentration of 20 μg was prepared, and a 5 μL drop was placed into a filter paper and imaged for fluorescence intensity.

particles/mL) had the highest particle concentration followed by HEB Organics (3.6×10^{12} particles/mL), Great Value (2.5×10^{12} particles/mL), HEB Brand (2.5×10^{12} particles/mL) milks, and the one with the lowest particle concentration was the Dairy Pure milk (8.2×10^{12} particles/mL) (Figure 1C).

Results obtained from Figure 1 clearly indicate that Horizon milk showed the ideal particle size and surface charge among all tested milk brands, having the highest particle concentration. Herein, to further confirm the ideal fat percentage required to achieve the ideal exosomes to serve as carriers to deliver NIR dye for bioimaging purposes, we chose four different grades of fat containing milk products of Horizon milk (0%, 1%, 2% and whole milk). The obtained particle size, zeta potential, and particle concentration of milk exosomes are presented in Figure 2. Fat free milk (0%) had an average particle size of 117.8 ± 6.76 nm, 1% milk resulted in an average particle size of 173.3 ± 7.73 nm, 2% fat milk had an average particle size of 260.5 ± 1.84 nm, and whole milk had a particle size average of 273.3 ± 8.12 nm. The zeta potential and particle concentration for the fat percentages were as follows for these samples: fat free milk (0%), ∼ −15 mV and 5.5×10^9 particles/mL; 1% milk, ∼ −14 mV and 3.3×10^9 particles/mL; 2% milk, ∼ −15 mV and 5.7×10^9 particles/mL; and whole milk, ∼ −14 mV and 8.2×10^{09} particles/mL. These results confirmed the selection of fat free milk for further analysis.

Physical Stability of Bovine Milk Exosomes

It is imperative to assess the stability of these exosomes or delivery vehicles under different physical conditions before

https://doi.org/10.1021/cbmi.4c00040
Chem. Biomed. Imaging 2024, 2, 711−720

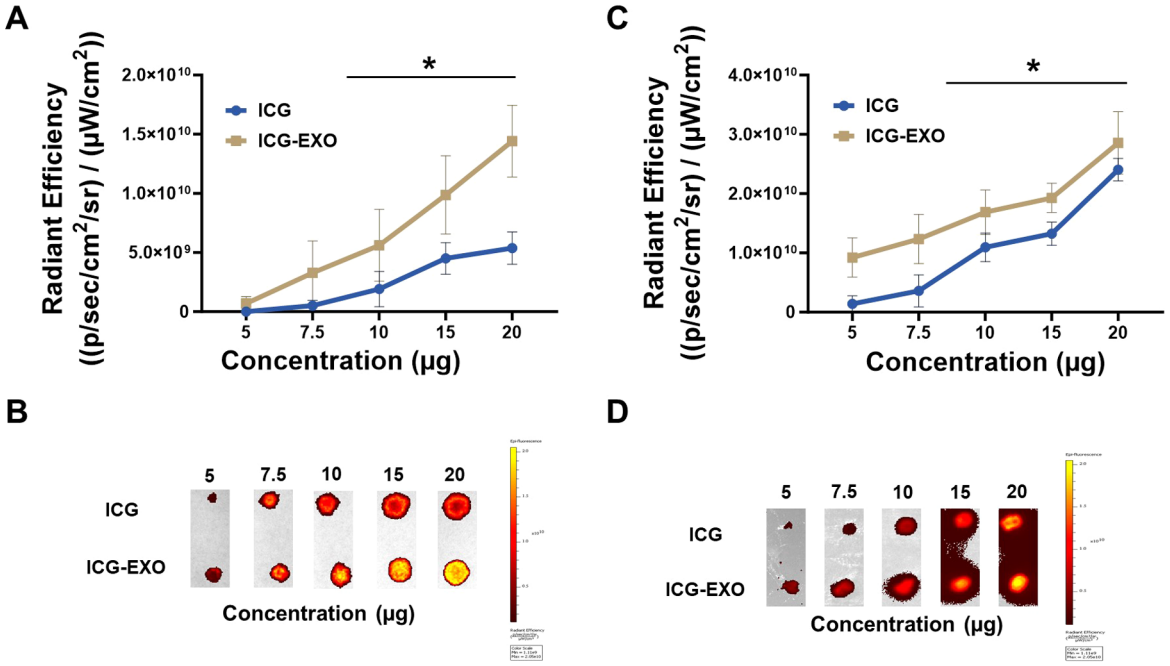

Figure 5. Comparison of radiant efficiency between ICG and ICG-EXO at different concentrations. (A) Fluorescence was measured using the IVIS imaging system at 5, 7.5, 10, 15, and 20 μg concentrations; line graphs represent the quantitative analysis of fluorescence signals/intensity ROI (radiation efficiency = photons/s/cm^2/sr). Data represents the average of three individual experiments. Error bars show SEM, $n = 3$. *$p < 0.05$. (B) A 5 μL drop of different concentrations was placed on filter paper and imaged right away. ICG loaded exosomes exhibited higher fluorescence when compared with free dye. (C) Fluorescence of dye and its loaded exosomes was measured using an IVIS imaging system at different concentrations. The quantitative analysis of fluorescence signals/intensity ROI (radiation efficiency = photons/s/cm^2/sr). Line graphs represent the average of three experiments. Error bars show SEM, $n = 3$. *$p < 0.05$. (D) A 5 μL drop of various concentrations was placed on top of a chicken breast tissue and imaged after 24 h for fluorescence measurement.

testing them *in vitro* and *in vivo* for biomedical applications. The changed behavior of the exosomal nanoparticles under certain environmental conditions were examined using the DLS system by measuring particle size after modifying pH, NaCl concentration (salinity), and temperature (Figure 3). In the case of pH, there is an increase in particle size at a pH of 2; this suggests that the exosome structure may be disassociating. On the other hand, when the pH is 6 or higher, there is a slight decrease in exosome size, suggesting that a high pH (6 or above) helps to stabilize the exosomal structure (Figure 3A). Regarding NaCl concentration, exosomal size increased after reaching 0.75%, the greatest particle size was observed when the NaCl concentration was at 1.00%. This shows that increasing NaCl destabilizes the exosomes after 0.50% NaCl. Anything below 0.50% NaCl showed a particle size similar to that of the control group, meaning that the stability of the nanoparticle was not affected (Figure 3B). The exosomes showed a slight increase in particle size at 37 °C and also showed a slight decrease at 25 °C; the other temperature ranges showed exosomes having around the same size, indicating that the exosomes are stable at most temperatures (Figure 3C).

Characterization of ICG dye loaded bovine milk exosomes

A schematic representation of the preparation (Figure 4A) and characterization (Figure 4B–E) of ICG-EXO is depicted below. The characterization of ICG-EXO formulation was determined by analyzing its particle size and concentration, surface charge, spectral analysis, and fluorescence intensity by utilizing various instruments such as a DLS instrument, spectrophotometer, and fluorescent animal imager, respectively.

DLS data revealed that ICG-EXO NPs had an average particle size of 92.89 ± 2.1 nm, particle concentration of ~2.67 × 10^{12}, and zeta potential (surface charge) of −13 ± 1.8 mV (Figure 4B). Next, UV–vis spectral analysis indicated that, with an increase of concentration, the absorbance peaks of ICG-EXO were enhanced. Absorbance peaks were mainly obtained around 720 nm (Figure 4B). To determine the fluorescence radiant efficiency of free ICG and ICG-EXO, nanoparticles were prepared at a final concentration of 20 μg. There was a significant difference between free dye and dye loaded exosomes as ICG free dye (5.4 × 10^9 RFU) showed a significantly lower radiance efficiency when compared with ICG loaded exosomes (1.4 × 10^{10} RFU) (Figure 4C). Next, Figure 4D demonstrates the qualitative representation of radiant efficiencies obtained for free ICG and its loaded exosomes.

Bovine Milk Exosomes Promote NIRF Imaging Characteristics

For NIRF imaging experiments, ICG and ICG-EXO were prepared at different concentrations for evaluating their concentration dependency. The radiant efficiency of Exo-Glow nanoformulation was measured using IVIS imaging system at different concentrations of 5, 7.5, 10, 15, and 20 μg by placing 5 μL drops on the filter paper (Figure 5A,B) and chicken breast (Figure 5C,D). The filter paper measurements were taken instantly, and results showed that the Exo-Glow nanoformulation had a higher fluorescence than the free dyes at all concentrations. The greatest difference was observed when comparing the highest concentration of 20 μg where ICG-EXO (1.4 × 10^{10} RFU) significantly surpassed free ICG (5.4 × 10^9 RFU) dye fluorescence (Figure 5A,B). For *ex vivo*

https://doi.org/10.1021/cbmi.4c00040
Chem. Biomed. Imaging 2024, 2, 711–720

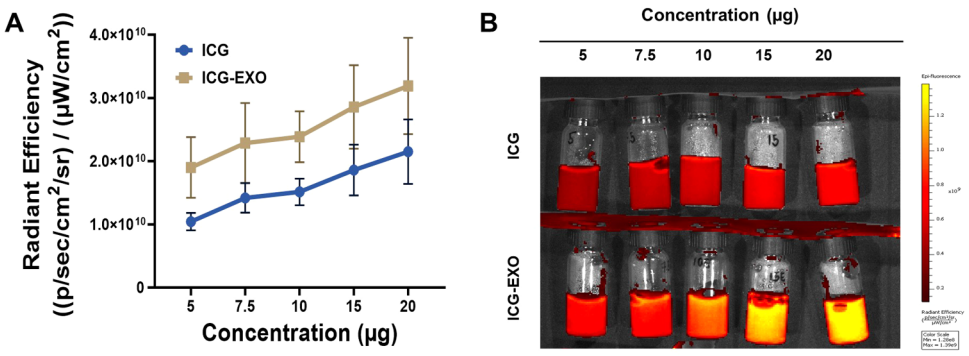

Figure 6. ICG-EXO exhibits superior tissue fluorescence contrast at different concentrations. (A) Fluorescence was measured using the IVIS imaging system at 5, 7.5, 10, 15, and 20 μg concentrations in agarose solution; line graphs represent the quantitative analysis of fluorescence signals/intensity ROI (radiation efficiency = photons/s/cm^2/sr). Data represents the average of three individual experiments. Error bars show SEM, n = 3. *p < 0.05. (B) Visualization of different concentrations of ICG and ICG-EXO in glass vials.

bioimaging, the chicken breast showed a similar pattern where Exo-Glow NPs (ICG-EXO - 2.9 × 10^{10} RFU) showed a higher fluorescence when compared with free dye (ICG - 2.4 × 10^{10} RFU) at the highest concentration of 20 μg (Figure 5C,D) after 24 h of treatment incubation. It was evident in both experimental settings that fluorescence intensities were concentration dependent.

The stability of ICG dye and ICG-EXO in tissue mimicking conditions was evaluated (Figure 6). The data confirm a dose dependent fluorescence potential for free dye (Figure 6A) and formulation (Figure 6B). However, there is a clear evidence that an improved dose dependent fluorescence glow for ICG-EXO indicates its superior NIRF imaging capabilities.

ICG-EXO Demonstrates Cellular Compatibility

It is important to evaluate the hemocompatibility of nanoformulations to assess their preclinical and clinical utility. Herein, we carried out a hemolysis (blood cell toxicity) assay for our ICG dye loaded exosomal nanoformulation at different concentrations. Our results indicated that red blood cells, treated with free dye and ICG-EXO, did not show any signs of toxicity as compared with PBS as the negative control and SDS as the positive control (Figure 7A). This information supports the use of this NIR dye based nanoformulation for biomedical purposes. After evaluating the hemocompatibility of ICG-EXO, we were interested in determining the biocompatibility of ICG-EXO with cancer cells. For this, we employed an MTS assay, using MCF-7 breast cancer cells treated with various concentrations of ICG and ICG-EXO ranging from 5 to 200 μg for 24 h. It was clearly apparent in the cellular viability data that ICG-EXO was as biocompatible (minimal to no toxicity) as free ICG with all concentrations (Figure 7B). Together, these results indicated the safe use of ICG-EXO in preclinical settings.

ICG-EXO Exhibits Superior Cancer Cells and Tissue Imaging

Successful *ex vivo* bioimaging of ICG-EXO with chicken breast tissues encouraged us to explore the binding and imaging affinity of these NPs with cancer cells and tissues (Figure 8) since ICG exhibited higher fluorescence intensity and retention after 24 h in this tissue bioimaging.

For *in vitro* imaging of cancer cells, we incubated 2 breast cancer cell lines (MCF-7 and MDA-MB 231) with a 10 μg concentration for 24 h. Images appeared to have a significant increase in fluorescence intensity with ICG-EXO when compared with free ICG in both cell lines. Cells with no treatment served as the control (Figure 8A). The quantified fluorescence signal intensity data for both cell lines are represented in Figure 8B where ICG-EXO was ∼5 and ∼3 times higher than free ICG in MCF-7 and MDA-MB 231 cell lines, respectively.

Further, human breast cancer tissue microarrays were utilized to examine *in situ* tissue binding and imaging efficacy of ICG-EXO with 100 μg concentration (considering thick tissue density in tumors) (Figure 9).

The NIR fluorescence signals of ICG and ICG-EXO are negligible in normal breast tissues, whereas ICG-EXO fluorescent imaging signal from tumor tissues revealed preferential and significantly enhanced binding affinity toward malignant breast tumor tissues (Figure 9B) when compared with normal breast tissues (Figure 9A). This indicates that the ICG-EXO fluorescence signal is positive for tumor tissues. At the same time, fluorescence signals were found to be more intense with ICG-EXO than with free ICG. In addition, most of the tumor tissue fields are evidently labeled by ICG-EXO. Figure 9C further demonstrates the quantified fluorescence signal intensities of TMAs where ICG-EXO was ∼4 times higher than free ICG in malignant tumor cores.

DISCUSSION

Bovine milk is an abundant source of extracellular vesicles, including exosomes.[23] Milk exosomes can be considered as an alternative to cell-derived exosomes and can potentially serve as a platform for more personalized drug delivery. This is due to their cost effectiveness, enhanced biocompatibility, low toxicity, high specificity, and stability in acidic environments.[30,31] Milk derived exosomes are reported to be intrinsically stable combating the harsh and degrading gut environment which further enhances the exosomes' bioavailability by facilitating their absorption in systemic circulation.[32] In addition, since milk is a highly consumed beverage in humans, milk derived exosomes show the ability to bypass the clearance from an extreme surge of the immune system.[32] Many studies confirmed that bovine milk exosomes are employed as a nanocarrier or as a potential cancer biomarker.[33] Exosomes can potentially be used for delivery of agents using loading methods as electroporation and chemical transfection.[31] Bovine milk-derived exosomes have also been used to enhance the delivery of anticancer agents.[14,34] There are some studies that also explore the application of milk exosomes

https://doi.org/10.1021/cbmi.4c00040
Chem. Biomed. Imaging 2024, 2, 711−720

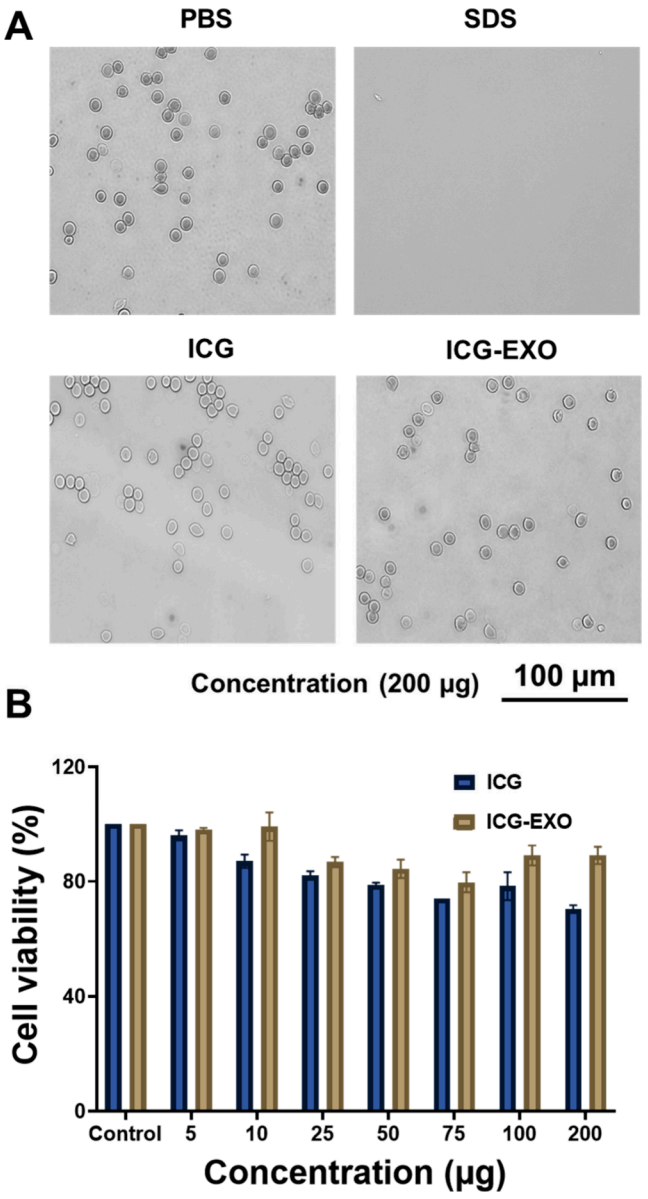

Figure 7. Cellular compatibility of ICG-EXO. (A) Human red blood cells were treated with a concentration of 200 μg of free ICG and ICG-EXO for 2 h. Microscopic images were captured to visualize hemolysis (hemocompatibility). PBS and SDS were used as negative and positive controls, respectively. Images are representative of triplicates. Images were taken at 200×. (B) Cell viability was measured with an MTS cell proliferation assay, using MCF-7 breast cancer cells after 24 h of treatment with different concentrations of ICG-EXO and its control free ICG. Absorbance was taken at 490 nm after incubating cells for 4 h with MTS reagent to determine cellular biocompatibility. Data was normalized to nontreated cells which served as controls in this experiment. Error bars show SEM, $n = 3$. *$p < 0.05$.

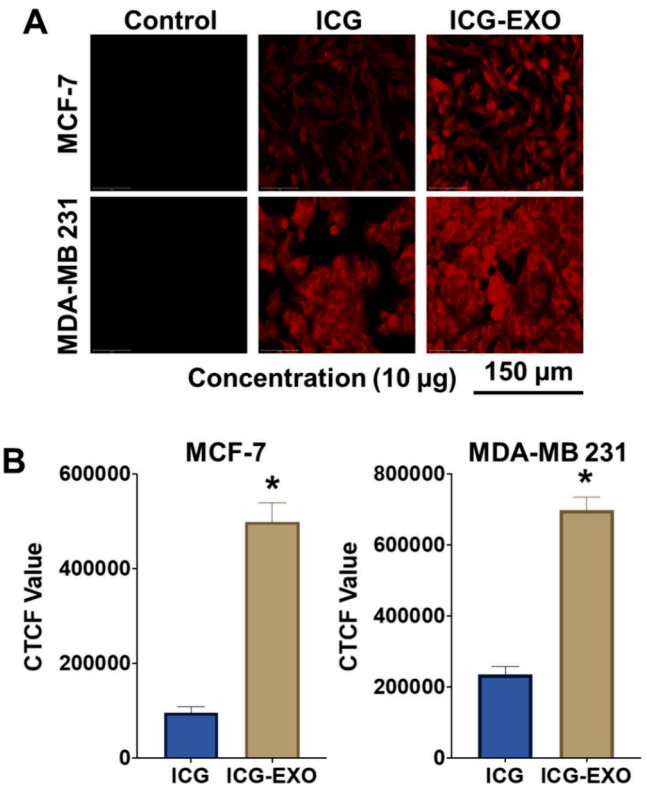

Figure 8. ICG-EXO exhibits superior breast cancer cell binding. (A) MCF-7 and MDA-MB-231 breast cancer cell lines were treated with ICG-EXO and its free dye control for 24 h with 10 μg concentration. Cells were then fixed and imaged with a fluorescent microscope. Images were taken at 200×. (B) Bar graphs represent the average quantification of three individual experiments as CTCF values (corrected total cell fluorescence). Error bars show SEM, $n = 3$. *$p < 0.05$.

in metabolism and health, and as genomic markers.[35] However, there is a limited number of articles discussing its potential as a dye or imaging agent carrier.

In this study, we utilized acetic acid treatment for exosome purification, which resulted in casein aggregation and isoelectric precipitation to facilitate efficient isolation of more purified exosomes. The obtained results (Figures 1−3) agree with literature that bovine milk exosome use in human medicine is much feasible.[23] The acetic acid extraction method can be an even more useful technique for the isolation and production of exosomes on a larger scale.[24] Previous studies have shown that lowering the pH can lead to purer and a higher number of exosomes,[36] but they also suggested the degradation of EV-surface-marker proteins after the acidification process.[24] Our study showed that these exosomes have a good physical stability at different temperatures, as well as in high pH medium conditions (Figure 3A, B). In addition, they were stable at low NaCl concentrations (Figure 3C).

Enhanced deep tissue penetration and low interference with fluorescence from tissue and biological samples make NIR dyes an excellent tool for bioimaging. Many significant efforts have been made toward developing such imaging agents that excites in near-infrared region including cyanine, squaraine, xanthenes and many others which often are linked with photobleaching and stability, solubility and aggregation issues.[5] Despite all these efforts, ICG is the only FDA approved NIR agent that is available for clinical use; however, ICG has also been reported to have rapid hepatic clearance, poor photostability, and concentration dependent aggregation.[37] In addition, ICG internalization is not organ/cancer specific.[38,39] Herein, this study aims at resolving these issues and obstacles associated with the use of NIR agents by developing and characterizing extracellular vesicle-based natural nanosystems to load and deliver NIR dye.

There are a variety of techniques to encapsulate the dyes/imaging agents into the exosomes.[40−42] In this study, the

https://doi.org/10.1021/cbmi.4c00040
Chem. Biomed. Imaging 2024, 2, 711−720

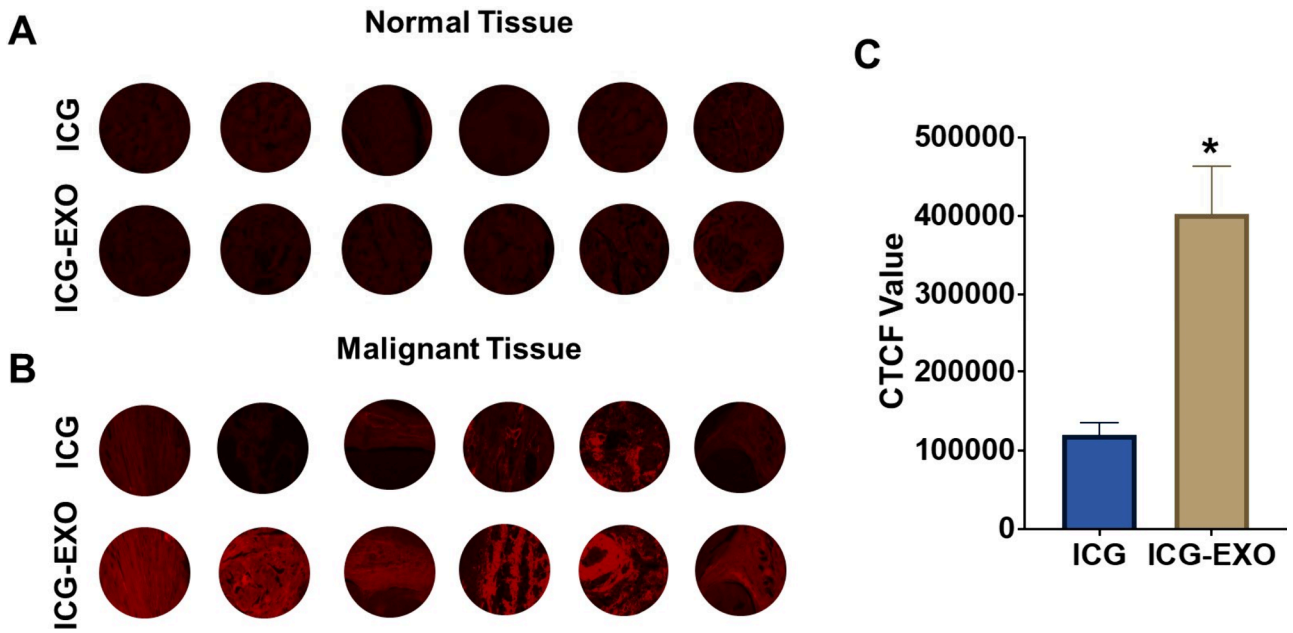

Figure 9. ICG-EXO demonstrates improved breast cancer tissue specific binding. The binding affinity of ICG loaded exosomal NPs was examined with (A) breast normal tissue and (B) human breast cancer tissue in microarrays. TMAs were processed for imaging after an overnight incubation with ICG-EXO and its equivalent free ICG at 100 μg. NPs showed significantly higher fluorescence signal and/or binding affinity with cancerous tissues than free ICG. Images were taken at 40×. (C) Quantitative analysis (CTCF values) of the fluorescence signals of the TMA cores. Error bars show SEM, *$p < 0.05$.

sonication procedure was employed because it can maintain the integrity of the exosome nanoparticle/lipid structure and can further improve the stability (Figure 4). The developed ICG-EXO formulation exhibited superior NIRF imaging characteristics on tissue paper, chicken tissue, and 2% agarose solution (Figures 4–6). In addition, ICG-EXO formulation is biocompatible, showing no effect on red blood cell morphology and no significant influence on cell viability of MCF-7 cells (Figure 7).

Various reports have suggested that milk exosomes can be useful nanocarriers due to their structure and origin.[43,44] This is also due to its composition of mRNAs, miRNA, and proteins.[45,46] ICG has been widely utilized for tumor labeling, visualization, and targeting.[47−50] Our study results confirm that milk exosomes not only are able to carry ICG (ICG-EXO) but also exhibit intense detection or glow of cancer cells (Figure 8) and tumor cell specific labeling of breast cancer tissues (Figure 9). However, further studies are warranted to fully establish this Exo-Glow platform for its imaging applicability in biomedical settings.

CONCLUSION

This study developed a fast and effective procedure for the milk exosome based ICG probe ICG-EXO. The developed ICG-EXO has the potential to improve solubility, photostability, and biocompatibility. The utility of ICG-EXO for effective NIR fluorescence cell and tissue imaging is confirmed. These promising results suggest the ability of ICG-EXO as a safer NIR imaging tool for cancer cells/tissues and pave the ways for its implications in tumor visualization.

AUTHOR INFORMATION

Corresponding Author

Murali M. Yallapu − *Division of Immunology and Microbiology, Medicine and Oncology Integrated Service Unit, School of Medicine, The University of Texas Rio Grande Valley, McAllen, Texas 78504, United States; South Texas Center of Excellence in Cancer Research, School of Medicine, University of Texas Rio Grande Valley, McAllen, Texas 78504, United States;* orcid.org/0000-0002-0073-8828; Phone: +1 (956) 296 1734; Email: murali.yallapu@utrgv.edu

Authors

Nycol M. Cotto − *Division of Immunology and Microbiology, Medicine and Oncology Integrated Service Unit, School of Medicine, The University of Texas Rio Grande Valley, McAllen, Texas 78504, United States; South Texas Center of Excellence in Cancer Research, School of Medicine, University of Texas Rio Grande Valley, McAllen, Texas 78504, United States*

Neeraj Chauhan − *Division of Immunology and Microbiology, Medicine and Oncology Integrated Service Unit, School of Medicine, The University of Texas Rio Grande Valley, McAllen, Texas 78504, United States; South Texas Center of Excellence in Cancer Research, School of Medicine, University of Texas Rio Grande Valley, McAllen, Texas 78504, United States;* orcid.org/0000-0001-6215-7132

Benilde Adriano − *Division of Immunology and Microbiology, Medicine and Oncology Integrated Service Unit, School of Medicine, The University of Texas Rio Grande Valley, McAllen, Texas 78504, United States; South Texas Center of Excellence in Cancer Research, School of Medicine, University of Texas Rio Grande Valley, McAllen, Texas 78504, United States*

Deepak S. Chauhan − *Division of Immunology and Microbiology, Medicine and Oncology Integrated Service Unit, School of Medicine, The University of Texas Rio Grande Valley, McAllen, Texas 78504, United States; South Texas Center of Excellence in Cancer Research, School of*

https://doi.org/10.1021/cbmi.4c00040
Chem. Biomed. Imaging 2024, 2, 711−720

Medicine, University of Texas Rio Grande Valley, McAllen, Texas 78504, United States

Marco Cabrera − *Division of Immunology and Microbiology, Medicine and Oncology Integrated Service Unit, School of Medicine, The University of Texas Rio Grande Valley, McAllen, Texas 78504, United States; South Texas Center of Excellence in Cancer Research, School of Medicine, University of Texas Rio Grande Valley, McAllen, Texas 78504, United States*

Subhash C. Chauhan − *Division of Immunology and Microbiology, Medicine and Oncology Integrated Service Unit, School of Medicine, The University of Texas Rio Grande Valley, McAllen, Texas 78504, United States; South Texas Center of Excellence in Cancer Research, School of Medicine, University of Texas Rio Grande Valley, McAllen, Texas 78504, United States*

Complete contact information is available at: https://pubs.acs.org/10.1021/cbmi.4c00040

Author Contributions

[§]N.M.C. and N.C. contributed equally to this work. Conceptualization, M.M.Y.; methodology, N.M.C., B.A., D.S.C., N.C.; software, N.M.C., N.C., M.M.Y.; validation, N.C., M.J., S.C.C., M.M.Y.; formal analysis, N.C., M.M.Y.; investigation, N.M.C., B.A., D.S.C., N.C.; resources, M.J., S.C.C., M.M.Y.; data curation N.M.C., N.C., M.M.Y.; writing—original draft preparation, N.M.C., N.C., M.M.Y.; writing-review and editing, N.M.C., N.C., M.J., S.C.C., M.M.Y; visualization, N.M.C., B.A., N.C., M.C., M.M.Y.; supervision, M.M.Y.; project administration, M.M.Y.; funding acquisition, S.C.C., M.M.Y. All authors have read and agreed to the published version of the manuscript.

Notes

The authors declare no competing financial interest.

■ ACKNOWLEDGMENTS

This research was partially supported by Start-up from Division of Immunology and Microbiology, Medicine and Oncology ISU, School of Medicine, University of Texas Rio Grande Valley and NIH grants (SC1GM139727, R01 CA210192, and R01 CA206069). This research work utilized equipment and services of Integrated Cancer Research Center funded by CPRIT (RP210180 and RP230419) and UT System Star Award.

■ REFERENCES

(1) Hilderbrand, S. A; Weissleder, R. Near-infrared fluorescence: application to in vivo molecular imaging. *Current Opinion in Chemical Biology* **2010**, *14* (1), 71−79.

(2) Pysz, M. A.; Gambhir, S. S.; Willmann, J. K. J. C. r. *Molecular imaging: current status and emerging strategies* **2010**, *65* (7), 500−516.

(3) Frangioni, J In vivo near-infrared fluorescence imaging. *Current Opinion in Chemical Biology* **2003**, *7* (5), 626−634.

(4) Luo, S.; Zhang, E.; Su, Y.; Cheng, T.; Shi, C. A review of NIR dyes in cancer targeting and imaging. *Biomaterials* **2011**, *32* (29), 7127−7138.

(5) Escobedo, J. O.; Rusin, O.; Lim, S.; Strongin, R. M. NIR dyes for bioimaging applications. *Curr. Opin. Chem. Biol.* **2010**, *14* (1), 64−70.

(6) Boni, L.; David, G.; Mangano, A.; Dionigi, G.; Rausei, S.; Spampatti, S.; Cassinotti, E.; Fingerhut, A. Clinical applications of indocyanine green (ICG) enhanced fluorescence in laparoscopic surgery. *Surgical endoscopy* **2015**, *29* (7), 2046−55.

(7) Sheng, Z.; Hu, D.; Xue, M.; He, M.; Gong, P.; Cai, L. Indocyanine Green Nanoparticles for Theranostic Applications. *Nano-Micro Letters* **2013**, *5* (3), 145−150.

(8) Wang, X.; Ku, G.; Wegiel, M. A.; Bornhop, D. J.; Stoica, G.; Wang, L. V. Noninvasive photoacoustic angiography of animal brains in vivo with near-infrared light and an optical contrast agent. *Optics letters* **2004**, *29* (7), 730−2.

(9) Wang, Y.-W.; Fu, Y.-Y.; Peng, Q.; Guo, S.-S.; Liu, G.; Li, J.; Yang, H.-H.; Chen, G.-N. Dye-enhanced graphene oxide for photothermal therapy and photoacoustic imaging. *J. Mater. Chem. B* **2013**, *1* (42), 5762−5767.

(10) Bishnoi, S.; Rehman, S.; Dutta, S. B.; De, S. K.; Chakraborty, A.; Nayak, D.; Gupta, S. Optical-Property-Enhancing Novel Near-Infrared Active Niosome Nanoformulation for Deep-Tissue Bioimaging. *ACS Omega* **2021**, *6* (35), 22616−22624.

(11) Kahlert, C.; Kalluri, R. J. J. o. m. m. *Exosomes in tumor microenvironment influence cancer progression and metastasis* **2013**, *91* (4), 431−437.

(12) Raposo, G.; Stoorvogel, W. J. J. o. C. B. Extracellular vesicles: exosomes, microvesicles, and friends. *J Cell Biol.* **2013**, *200* (4), 373−383.

(13) Théry, C.; Zitvogel, L.; Amigorena, S. J. N. r. i. *Exosomes: composition, biogenesis and function* **2002**, *2* (8), 569−579.

(14) Adriano, B.; Cotto, N. M.; Chauhan, N.; Jaggi, M.; Chauhan, S. C.; Yallapu, M. M. Milk exosomes: Nature's abundant nanoplatform for theranostic applications. *Bioactive Materials* **2021**, *6* (8), 2479−2490.

(15) Turturici, G.; Tinnirello, R.; Sconzo, G.; Geraci, F. Extracellular membrane vesicles as a mechanism of cell-to-cell communication: advantages and disadvantages. *American Journal of Physiology-Cell Physiology* **2014**, *306* (7), C621−C633.

(16) Ju, S.; Mu, J.; Dokland, T.; Zhuang, X.; Wang, Q.; Jiang, H.; Xiang, X.; Deng, Z.-B.; Wang, B.; Zhang, L.; et al. Grape exosome-like nanoparticles induce intestinal stem cells and protect mice from DSS-induced colitis. *Mol. Ther.* **2013**, *21* (7), 1345−1357.

(17) Zhang, M.; Viennois, E.; Xu, C.; Merlin, D. J. T. b. *Plant derived edible nanoparticles as a new therapeutic approach against diseases* **2016**, *4* (2), No. e1134415.

(18) Hata, T.; Murakami, K.; Nakatani, H.; Yamamoto, Y.; Matsuda, T.; Aoki, N. J. B. *communications, b. r., Isolation of bovine milk-derived microvesicles carrying mRNAs and microRNAs* **2010**, *396* (2), 528−533.

(19) Izumi, H.; Kosaka, N.; Shimizu, T.; Sekine, K.; Ochiya, T.; Takase, M. J. J. o. d. s. *Bovine milk contains microRNA and messenger RNA that are stable under degradative conditions* **2012**, *95* (9), 4831−4841.

(20) Reinhardt, T. A.; Lippolis, J. D.; Nonnecke, B. J.; Sacco, R. E. Bovine milk exosome proteome. *Journal of proteomics* **2012**, *75* (5), 1486−92.

(21) Samuel, M.; Chisanga, D.; Liem, M.; Keerthikumar, S.; Anand, S.; Ang, C.-S.; Adda, C. G.; Versteegen, E.; Jois, M.; Mathivanan, S. Bovine milk-derived exosomes from colostrum are enriched with proteins implicated in immune response and growth. *Sci. Rep.* **2017**, *7* (1), 5933.

(22) Escudier, B.; Dorval, T.; Chaput, N.; André, F.; Caby, M. P.; Novault, S.; Flament, C.; Leboulaire, C.; Borg, C.; Amigorena, S.; Boccaccio, C.; Bonnerot, C.; Dhellin, O.; Movassagh, M.; Piperno, S.; Robert, C.; Serra, V.; Valente, N.; Le Pecq, J. B.; Spatz, A.; Lantz, O.; Tursz, T.; Angevin, E.; Zitvogel, L. Vaccination of metastatic melanoma patients with autologous dendritic cell (DC) derived-exosomes: results of thefirst phase I clinical trial. *Journal of translational medicine* **2005**, *3* (1), 10.

(23) Yamauchi, M.; Shimizu, K.; Rahman, M.; Ishikawa, H.; Takase, H.; Ugawa, S.; Okada, A.; Inoshima, Y. Efficient method for isolation of exosomes from raw bovine milk. *Drug Dev. Ind. Pharm.* **2019**, *45* (3), 359−364.

(24) Rahman, M. M.; Shimizu, K.; Yamauchi, M.; Takase, H.; Ugawa, S.; Okada, A.; Inoshima, Y. Acidification effects on isolation of extracellular vesicles from bovine milk. *PLoS One* **2019**, *14* (9), No. e0222613.

(25) Bickmore, D. C.; Miklavcic, J. J. Characterization of Extracellular Vesicles Isolated From Human Milk Using a Precipitation-Based Method. *Frontiers in nutrition* **2020**, *7*, 22.
(26) Chauhan, S. S.; Shetty, A. B.; Hatami, E.; Chowdhury, P.; Yallapu, M. M. Pectin-Tannic Acid Nano-Complexes Promote the Delivery and Bioactivity of Drugs in Pancreatic Cancer Cells. *Pharmaceutics* **2020**, *12* (3), 285.
(27) Li, Y.; Xing, L.; Wang, L.; Liu, X.; Wu, L.; Ni, M.; Zhou, Z.; Li, L.; Liu, X.; Huang, Y. Milk-derived exosomes as a promising vehicle for oral delivery of hydrophilic biomacromolecule drugs. *Asian Journal of Pharmaceutical Sciences* **2023**, *18* (2), No. 100797.
(28) Wang, M.; Lv, C.-Y.; Li, S.-A.; Wang, J.-K.; Luo, W.-Z.; Zhao, P.-C.; Liu, X.-Y.; Wang, Z.-M.; Jiao, Y.; Sun, H.-W.; Zhao, Y.; Zhang, P. Near infrared light fluorescence imaging-guided biomimetic nanoparticles of extracellular vesicles deliver indocyanine green and paclitaxel for hyperthermia combined with chemotherapy against glioma. *J. Nanobiotechnol.* **2021**, *19* (1), 210.
(29) Chauhan, N.; Cabrera, M.; Chowdhury, P.; Nagesh, P. K. B.; Dhasmana, A.; Pranav; Jaggi, M.; Chauhan, S. C.; Yallapu, M. M. Indocyanine Green-based Glow Nanoparticles Probe for Cancer Imaging. *Nanotheranostics* **2023**, *7* (4), 353−367.
(30) Melnik, B. C.; John, S. M.; Schmitz, G. Milk: an exosomal microRNA transmitter promoting thymic regulatory T cell maturation preventing the development of atopy? *Journal of translational medicine* **2014**, *12* (1), 43.
(31) Aqil, F.; Munagala, R.; Jeyabalan, J.; Agrawal, A. K.; Kyakulaga, A. H.; Wilcher, S. A.; Gupta, R. C. Milk exosomes - Natural nanoparticles for siRNA delivery. *Cancer letters* **2019**, *449*, 186−195.
(32) Samuel, M.; Fonseka, P.; Sanwlani, R.; Gangoda, L.; Chee, S. H.; Keerthikumar, S.; Spurling, A.; Chitti, S. V.; Zanker, D.; Ang, C.-S.; Atukorala, I.; Kang, T.; Shahi, S.; Marzan, A. L.; Nedeva, C.; Vennin, C.; Lucas, M. C.; Cheng, L.; Herrmann, D.; Pathan, M.; Chisanga, D.; Warren, S. C.; Zhao, K.; Abraham, N.; Anand, S.; Boukouris, S.; Adda, C. G.; Jiang, L.; Shekhar, T. M.; Baschuk, N.; Hawkins, C. J.; Johnston, A. J.; Orian, J. M.; Hoogenraad, N. J.; Poon, I. K.; Hill, A. F.; Jois, M.; Timpson, P.; Parker, B. S.; Mathivanan, S. Oral administration of bovine milk-derived extracellular vesicles induces senescence in the primary tumor but accelerates cancer metastasis. *Nat. Commun.* **2021**, *12* (1), 3950.
(33) Xu, L.; Wu, L.-F.; Deng, F.-Y. Exosome: An Emerging Source of Biomarkers for Human Diseases. *Current Molecular Medicine* **2019**, *19* (6), 387−394.
(34) Aqil, F.; Munagala, R.; Jeyabalan, J.; Agrawal, A. K.; Gupta, R. Exosomes for the Enhanced Tissue Bioavailability and Efficacy of Curcumin. *AAPS Journal* **2017**, *19* (6), 1691−1702.
(35) Cintio, M.; Polacchini, G.; Scarsella, E.; Montanari, T.; Stefanon, B.; Colitti, M. J. A. *MicroRNA Milk Exosomes: From Cellular Regulator to Genomic Marker* **2020**, *10* (7), 1126.
(36) Ban, J. J.; Lee, M.; Im, W.; Kim, M. Low pH increases the yield of exosome isolation. *Biochemical and biophysical research communications* **2015**, *461* (1), 76−9.
(37) Pauli, J.; Vag, T.; Haag, R.; Spieles, M.; Wenzel, M.; Kaiser, W. A.; Resch-Genger, U.; Hilger, I. An in vitro characterization study of new near infrared dyes for molecular imaging. *European journal of medicinal chemistry* **2009**, *44* (9), 3496−503.
(38) Mondal, S. B.; Gao, S.; Zhu, N.; Liang, R.; Gruev, V.; Achilefu, S. Chapter Five - Real-Time Fluorescence Image-Guided Oncologic Surgery. In *Adv. Cancer Res.*; Pomper, M. G.; Fisher, P. B., Eds.; Academic Press: 2014; Vol. *124*, pp 171−211.
(39) Veys, I.; Pop, C. F.; Barbieux, R.; Moreau, M.; Noterman, D.; De Neubourg, F.; Nogaret, J. M.; Liberale, G.; Larsimont, D.; Bourgeois, P. ICG fluorescence imaging as a new tool for optimization of pathological evaluation in breast cancer tumors after neoadjuvant chemotherapy. *PLoS One* **2018**, *13* (5), No. e0197857.
(40) Munagala, R.; Aqil, F.; Jeyabalan, J.; Gupta, R. C. Bovine milk-derived exosomes for drug delivery. *Cancer Letters* **2016**, *371* (1), 48−61.
(41) Sun, D.; Zhuang, X.; Xiang, X.; Liu, Y.; Zhang, S.; Liu, C.; Barnes, S.; Grizzle, W.; Miller, D.; Zhang, H.-G. A Novel Nanoparticle Drug Delivery System: The Anti-inflammatory Activity of Curcumin Is Enhanced When Encapsulated in Exosomes. *Molecular Therapy* **2010**, *18* (9), 1606−1614.
(42) Pascucci, L.; Coccè, V.; Bonomi, A.; Ami, D.; Ceccarelli, P.; Ciusani, E.; Viganò, L.; Locatelli, A.; Sisto, F.; Doglia, S. M.; Parati, E.; Bernardo, M. E.; Muraca, M.; Alessandri, G.; Bondiolotti, G.; Pessina, A. Paclitaxel is incorporated by mesenchymal stromal cells and released in exosomes that inhibit in vitro tumor growth: A new approach for drug delivery. *J. Controlled Release* **2014**, *192*, 262−270.
(43) Munagala, R.; Aqil, F.; Jeyabalan, J.; Gupta, R. C. Bovine milk-derived exosomes for drug delivery. *Cancer letters* **2016**, *371* (1), 48−61.
(44) Tominaga, N.; Yoshioka, Y.; Ochiya, T. A novel platform for cancer therapy using extracellular vesicles. *Advanced drug delivery reviews* **2015**, *95*, 50−5.
(45) Hata, T.; Murakami, K.; Nakatani, H.; Yamamoto, Y.; Matsuda, T.; Aoki, N. Isolation of bovine milk-derived microvesicles carrying mRNAs and microRNAs. *Biochemical and biophysical research communications* **2010**, *396* (2), 528−33.
(46) Izumi, H.; Kosaka, N.; Shimizu, T.; Sekine, K.; Ochiya, T.; Takase, M. Bovine milk contains microRNA and messenger RNA that are stable under degradative conditions. *Journal of dairy science* **2012**, *95* (9), 4831−4841.
(47) Sitia, L.; Sevieri, M.; Bonizzi, A.; Allevi, R.; Morasso, C.; Foschi, D.; Corsi, F.; Mazzucchelli, S. Development of Tumor-Targeted Indocyanine Green-Loaded Ferritin Nanoparticles for Intraoperative Detection of Cancers. *ACS Omega* **2020**, *5* (21), 12035−12045.
(48) Zheng, C.; Zheng, M.; Gong, P.; Jia, D.; Zhang, P.; Shi, B.; Sheng, Z.; Ma, Y.; Cai, L. Indocyanine green-loaded biodegradable tumor targeting nanoprobes for in vitro and in vivo imaging. *Biomaterials* **2012**, *33* (22), 5603−5609.
(49) Zheng, M.; Zhao, P.; Luo, Z.; Gong, P.; Zheng, C.; Zhang, P.; Yue, C.; Gao, D.; Ma, Y.; Cai, L. Robust ICG Theranostic Nanoparticles for Folate Targeted Cancer Imaging and Highly Effective Photothermal Therapy. *ACS Appl. Mater. Interfaces* **2014**, *6* (9), 6709−6716.
(50) Sevieri, M.; Silva, F.; Bonizzi, A.; Sitia, L.; Truffi, M.; Mazzucchelli, S.; Corsi, F. Indocyanine Green Nanoparticles: Are They Compelling for Cancer Treatment? *Frontiers in chemistry* **2020**, *8*, 535.

https://doi.org/10.1021/cbmi.4c00040
Chem. Biomed. Imaging 2024, 2, 711−720